https://doi.org/10.1016/j.isatra.2020.05.026

Stable Control of Magnetically Suspended Motor with Heavy Self-weight and Great Moment of Inertia

ABSTRACT

In this article, for the translation and radial rotation of the magnetically suspended motor (MSM) with heavy self-weight and great moment of inertia, robust control functions are designed to improve the disturbance attenuation by minimizing model uncertainties introduced by variations of current stiffness and displacement stiffness. On the one hand, the H_∞ control function with the mixed sensitivity is designed to the translational control of the MSM. On the other hand, for the rotation control of the MSM around radial axes, μ-synthesis is utilized to attenuate disturbances caused by the gyroscopic coupling with variable rotational speed. Simulation is developed to testify the disturbance attenuation of control functions when pulse-type, sinusoidal-type and random-type disturbances are imposed on the MSM respectively. Furthermore, experiments about axial translation and radial rotation are conducted to validate the robust stability of designed control functions. Both simulation and experimental results indicate that the robust control scheme has better ability on disturbance attenuation of the MSM with great inertia of moment and heavy self-weight.

Keywords--magnetically suspended motor; disturbance attenuation; robust control; current stiffness; displacement stiffness.

1. Introduction

The rotor in flywheel energy storage system (FESS) [1-3] has form of a big disc with great equatorial moment of inertia to generate large driving moment or to store a large amount of mechanical energy. Moreover, in order to improve the working efficiency and guarantee the stability of rotational machine when the rotor works at a high speed, some novel suspension and supporting ways such as gas bearing [4-6], oil film bearing [7, 8] and magnetic bearing [9-11] were applied in the rotational machinery. Especially, the active magnetic bearing (AMB) is promising to be used in the rotational machine because of its advantages on active controllability, non-contact friction, lubrication-free and long lifespan. There are many products of high speed rotational machinery using the AMB system, for example, the magnetically suspended flywheel for attitude control of satellite [12, 13], the magnetically suspended centrifugal compressor [14, 15] and the magnetically suspended vacuum pump [16-18]. Therefore, the stable control of magnetically suspended rotor is the research focus of the magnetically suspended

rotational machinery. In general, the proportional-integral-derivative (PID) control [19-21] was applied in the closed-loop control of MSM based on the displacement feedback. Other control methods such as the Kalman filter [22], the fuzzy control [23-25], the adaptive control [26, 27] and the sliding-mode control (SMC) [28-30] were reported in the control engineering of MSM as well. Aiming at further improving the ability on disturbance attenuation of the MSM, the robust control method was also proposed and tested in the practical control engineering. A high performance hybrid control scheme with a feedback H_∞ control and an inner-loop disturbance observer (DOB) was used to suppress constant and harmonic disturbances acting on the MSM at different rotational speeds [31, 32]. In a high-speed AMB spindle system, a μ-synthesis controller [33] was designed to minimize the error between the reference position and the estimated position, this method corrected the inability to measure real-time position in the presence of machining disturbance. In a three-pole AMB rotor system, the robust stabilization control using two stages of SMC was proposed to reduce the mismatch uncertainties due to the magnetic coupling and the actuator dynamics [34]. A robust controller [35] was designed for the active vibration control of radial homo-polar AMB rotor system, and experimental results showed that the control system had good performances on the transient response and the robustness. A robust fuzzy controller based on the Takagi-Sugeno fuzzy model was proposed for a nonlinear AMB system with time-varying parametric uncertainty [36], and it was more tractable and accessible. The H_∞ control was proposed to attenuate the disturbance in a flexible MSM system [37]. A controller with μ-synthesis based on the model incorporating uncertainty was designed in a horizontal MSM system [38], the limits of allowable parameter changes for robust stability were tested and established.

However, the model uncertainties caused by the variation of current stiffness and displacement stiffness in the MSM were not yet analyzed. In above-mentioned literatures, the displacement stiffness and the current stiffness are viewed as the constant values without influence of variable airgap and external disturbance. Especially, compared to the MSM with light self-weight, the controllable airgap in the heavy self-weight MSM easily deflect from the nominal equilibrium position when different loads are mounted on the MSM, and then the current stiffness and the displacement stiffness would deviate from the nominal values. Moreover, different initial positions of the MSM also lead to uncertainties of the current stiffness and the displacement stiffness in the practical situation. A transient displacement deflection possibly makes the current stiffness and the displacement stiffness deviate from the nominal values when the MSM is suffered from disturbances such as the wind drag at high speed and the self-excited vibration. More importantly, the unstable MSM rotor with heavy self-weight possibly generates great shock

on the stator part, and then the whole MSM system would be broken. So, the risk of unstable MSM rotor with heavy self-weight is raised with the rotational speed. Almost publications were focused on the static suspension control of the MSM, and the gyroscopic coupling of the MSM at dynamic rotation was not mitigated, but it could generate disturbance on the dynamic rotation control of the MSM.

Above all, compared to the MSM rotor in the above-mentioned references, the stable control of the MSM with heavy self-weight and great moment of inertia is still challenging, especially the MSM with heavy self-weight and great moment of inertia has variable rotational speed and indefinite initial suspension position. The stable control considering the variable rotational speed and indefinite initial suspension position is critical to improve the robust stability and the disturbance attenuation of the MSM with heavy self-weight and great moment of inertia. In this article, robust control functions are designed to the static suspension and dynamic rotation of the MSM rotor, so the robust stability of the MSM rotor is improved. Therefore, this robust control method is potential to be applied into the control engineering of the MSM rotor with a heavy self-weight and great moment of inertia, and the stable operational range of the MSM rotor with a heavy self-weight and great moment of inertia is expanded.

This article is organized as follows. The dynamic characteristics of the MSM rotor are studied in section 2. Furthermore, the robust control functions of translation and radial rotation are designed in section 3. Simulations about translation and radial rotation of the MSM rotor are conducted in section 4. Moreover, experiments are conducted to verify the effectiveness of designed control functions in section 5. Finally, the conclusion is given.

2. Rotor Characteristics of MSM

2.1. Structure of MSM

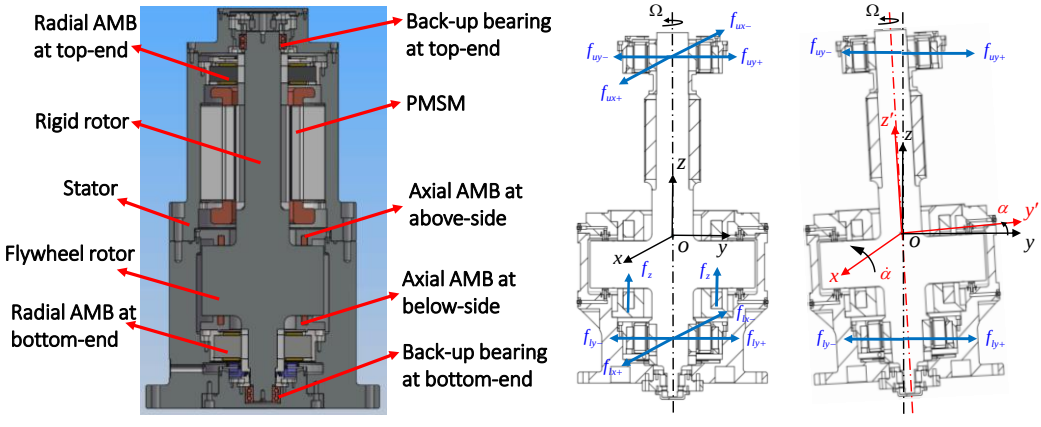

Fig. 1. (a) The structure of the MSM system, (b) balanced status, (c) tilting status.

The structure of MSM system is illustrated in Fig. 1(a), and it consists of a suspension system, a permanent magnet synchronous motor (PMSM) and a sensor system. The suspension system includes radial AMB, axial AMB

and back-up ball bearing. The radial AMB controls the radial motion of the MSM rotor, and the difference between magnetic forces of the radial AMBs at top-end and bottom-end generates torque to control the radial rotation of the MSM rotor. The axial AMB located at above-side and below-side of the flywheel rotor controls the stable suspension in axial direction. The back-up ball bearings at top-end and bottom-end secure the stability of the flywheel rotor when the magnetic suspension system fails to work or is switched off. The PMSM is the drive unit to control the rotation of the MSM rotor around the axial principal axis. The displacement sensors mounted on the stator part measure radial and axial displacement deflections of the MSM rotor.

2.2. Dynamic Equations of MSM Rotor

As illustrated in Fig. 1(b), the MSM rotor works at the balanced status with the function of magnetic forces generated by axial and radial AMBs. In radial direction, magnetic forces at top-end and bottom-end hold the MSM rotor to work at the equilibrium position. Axial magnetic forces generated by the axial AMB hold the MSM rotor to suspend at the axial equilibrium point. If there are external forces acting on the MSM rotor, it is possible that the MSM rotor would vibrate along three axes. For example, when the MSM rotor rotates around x axis with angle α in Fig. 1(c), the radial AMBs at top-end and bottom-end generate tilting torque to turn the MSM rotor back to the balanced position.

Considering the gravity of the MSM rotor, equations of translation along three axes are

$$\begin{cases} m\ddot{x} = f_x \\ m\ddot{y} = f_y \\ m\ddot{z} = f_z - mg \end{cases} \tag{1}$$

Equations of rotation around three axes are

$$\begin{cases} J_x\ddot{\alpha} + J_z\Omega\dot{\beta} = T_x \\ J_y\ddot{\beta} - J_z\Omega\dot{\alpha} = T_y \\ J_z\dot{\Omega} = T_z \end{cases} \tag{2}$$

where J_x=J_y is the equatorial moment of inertia, and J_z is the polar moment of inertia. α is the rotational angle around x axis, and β is the rotational angle around y axis. Ω is the rotational speed around z axis. T_x is tilting torque around x axis generated by the radial AMB in y axis, T_y is tilting torque around y axis generated by the radial AMB in x axis, T_z is the drive torque generated by the PMSM. For the symmetrical MSM rotor with suspension span l, tilting torques generated by radial AMBs at top-end and bottom-end are

$$\begin{cases} T_x = \left(f_{ux} + f_{lx} \right) \cdot l \\ T_y = \left(f_{uy} + f_{ly} \right) \cdot l \end{cases} \tag{3}$$

where f_{ux} is the magnetic force generated by radial AMB at top-end of x axis, f_{lx} is the magnetic force generated by radial AMB at bottom-end of x axis, f_{uy} is the magnetic force generated by radial AMB at top-end of y axis, f_{ly} is the magnetic force generated by radial AMB at bottom-end of y axis.

The relationship between radial displacement and rotational angle is

$$\begin{cases} \alpha = \dfrac{d_{y+} - d_{y-}}{l} \\ \beta = \dfrac{d_{x+} - d_{x-}}{l} \end{cases} \tag{4}$$

where d_{y+} is the displacement deflection of the MSM rotor along positive direction of y axis, d_{y-} is the displacement deflection of the MSM rotor along negative direction of y axis, d_{x+} is the displacement deflection of the MSM rotor along positive direction of x axis, d_{x-} is the displacement deflection of the MSM rotor along positive direction of x axis.

2.3. Magnetic Force of AMB System

The structure of radial AMB is illustrated in Fig. 2. There are four independent single-pole AMBs which generate magnetic forces to realize the active control of the MSM rotor. The equivalent magnet circuit of the radial AMB is shown in Fig. 2(b). The magnet flux generated by the winding of the radial AMB passes through stator, magnet ring, airgap and rotor, and equivalent reluctances of airgap and magnet ring. $R_{n=1-8}$, are in series connection within the same magnet pole in Fig. 2(c). N is the turn of winding, and $I_{n=1-8}$ is the control current of winding.

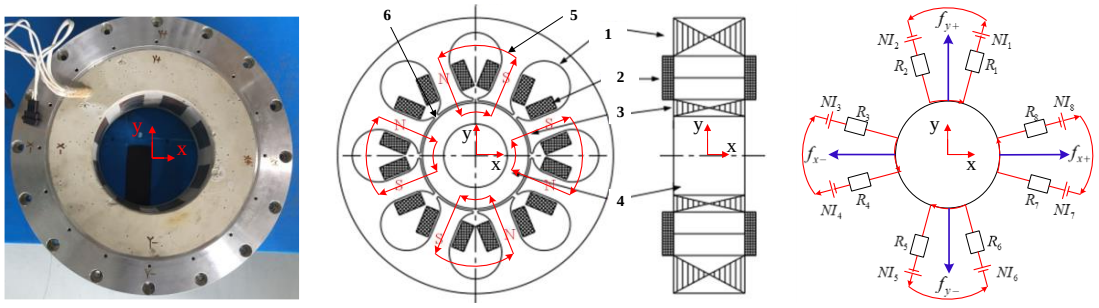

(a) (b) (c)

Fig. 2. The structure of the radial AMB, (a) prototype of radial AMB, (b) cross-sectional view (1--stator, 2--winding, 3--magnet ring, 4--rotor, 5--magnet flux, 6--airgap), (c) equivalent magnet circuit.

If there is no coupling effect among four radial AMBs, equivalent reluctances of four airgaps are expressed into respectively

$$\begin{cases} R_{y+} = R_1 + R_2 = \dfrac{2d_{y+}}{\mu_0 A_{y+}} & R_{y-} = R_5 + R_6 = \dfrac{2d_{y-}}{\mu_0 A_{y-}} \\ R_{x+} = R_7 + R_8 = \dfrac{2d_{x+}}{\mu_0 A_{x+}} & R_{x-} = R_3 + R_4 = \dfrac{2d_{x-}}{\mu_0 A_{x-}} \end{cases} \tag{5}$$

where $d_{n=x+,x-,y+,y-}$ is the length of airgap between rotor and stator. μ_0 is the vacuum permeability, and $A_{n=x+,x-,y+,y-}$ is the cross-sectional area of the magnet pole. The magnet flux in each airgap is

$$\begin{cases} \Phi_{y+} = \dfrac{NI_1 + NI_2}{R_1 + R_2} & \Phi_{y-} = \dfrac{NI_5 + NI_6}{R_5 + R_6} \\ \Phi_{x+} = \dfrac{NI_7 + NI_8}{R_7 + R_8} & \Phi_{x-} = \dfrac{NI_3 + NI_4}{R_3 + R_4} \end{cases} \tag{6}$$

The magnetic force is derived and written as

$$\begin{cases} f_{y+} = \dfrac{\Phi_{y+}^2}{\mu_0 A_{y+}} & f_{y-} = \dfrac{\Phi_{y-}^2}{\mu_0 A_{y-}} \\ f_{x+} = \dfrac{\Phi_{x+}^2}{\mu_0 A_{x+}} & f_{x-} = \dfrac{\Phi_{x-}^2}{\mu_0 A_{x-}} \end{cases} \tag{7}$$

The resultant magnetic force along x axis is expressed as

$$f(i_x, d_x) = f_{x+} - f_{x-} = \frac{\mu_0 A N^2}{4} \left[\frac{(I_0 + i_x)^2}{(d_0 - d_x)^2} - \frac{(I_0 - i_x)^2}{(d_0 + d_x)^2} \right] \tag{8}$$

where I_0 is the biased current, and i_x is the control current. The resultant magnetic force along y axis could be expressed similarly with the subscript y. The current stiffness k_i and the displacement stiffness k_d are expressed as

$$\begin{cases} k_i = \dfrac{\mu_0 A N^2 I_0}{d_0^2} \\ k_d = \dfrac{\mu_0 A N^2 I_0^2}{d_0^3} \end{cases} \tag{9}$$

Therefore, the uncertainties of the current stiffness and the displacement stiffness are introduced when the biased displacement d_0 and the cross-sectional area A deviate from their nominal values. In detail, the relations among the current stiffness, the displacement stiffness and the biased displacement are illustrated in Fig. 3. In radial direction, the nominal biased displacement sets at 1mm, and the deviation range is 0.2mm. The nominal value of radial current stiffness is 620N/A, and the nominal value of radial displacement stiffness is -2800N/mm. When the biased displacement deflects 0.1mm from the nominal value, the deflection value of radial current stiffness is about 100N/A as shown by the red-circle line in Fig. 3(a), and that of radial displacement stiffness is 1000N/mm in Fig. 3(b). Similarly, when the axial nominal biased displacement is 1.3mm with 0.2mm deviation range, the nominal value of axial current stiffness is 470N/A, and the nominal value of axial displacement stiffness

is -1700N/mm. If the axial biased displacement deflects 0.1mm from the equilibrium point, the deviation of axial current stiffness is 60N/A, and the deflection of axial displacement stiffness is 350N/mm.

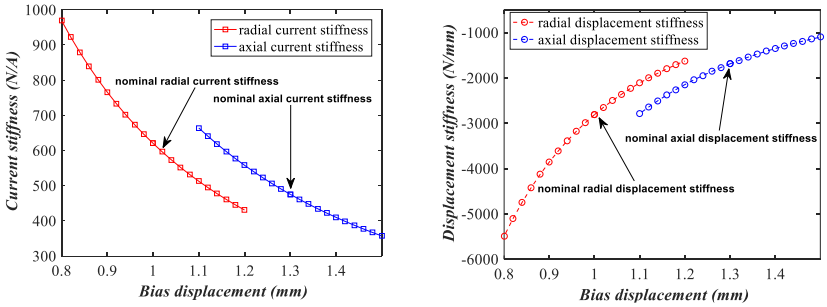

(a) (b)

Fig. 3. (a) Current stiffness versus biased displacement, (b) displacement stiffness versus biased displacement.

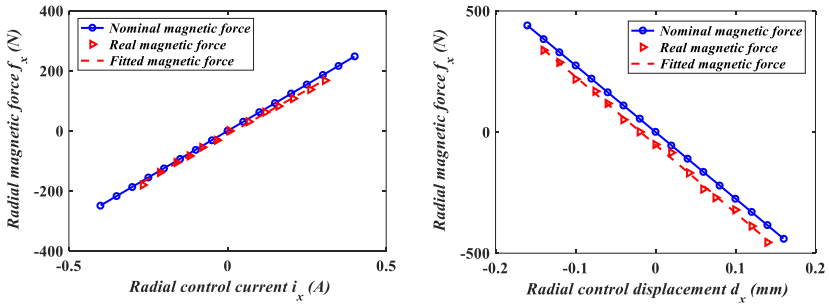

(a) (b)

Fig. 4. (a) Radial magnetic force versus control current, (b) radial magnetic force versus displacement.

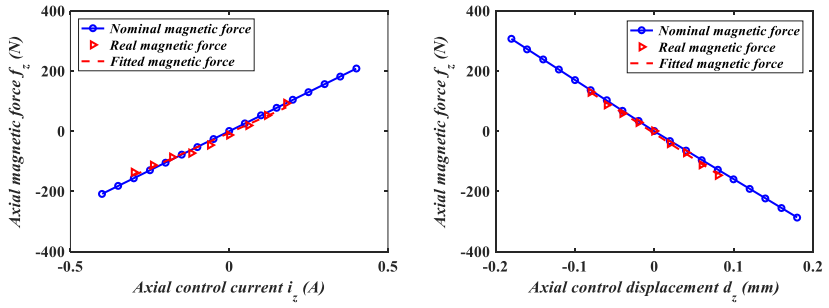

(a) (b)

Fig. 5. (a) Axial magnetic force versus control current, (b) axial magnetic force versus displacement.

For the radial magnetic force, the comparison between the calculated value and the measured value is shown in Fig. 4, the nominal value is plotted by the blue line, and the measured value is marked by the red line. The magnetic force is proportional to the control current and the control displacement within the vicinity of nominal airgap. In Fig. 4(b), the measured value of radial current stiffness is 608N/A, and the measured value of radial displacement stiffness is -2810N/mm. Moreover, as illuminated in Fig. 5, the measured value of axial current stiffness is 480N/A, and the measured value of axial displacement stiffness is -1702N/mm. Therefore, there is difference between the nominal value and the measured value, and then the various model uncertainties due to variations of the displacement stiffness and the current stiffness likely affect the stability of MSM rotor.

3. Control Function Design for MSM Rotor

3.1. Control Loop of Translation

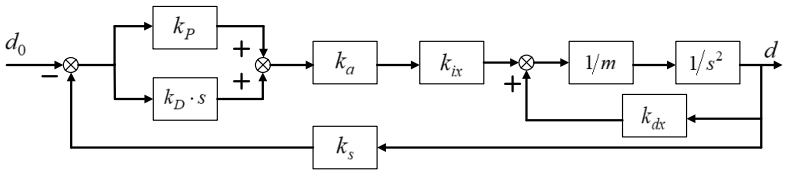

Fig. 6. The translation control scheme of the MSM rotor.

The translational control loop of the MSM rotor is shown in Fig. 6. The control system includes the stiffness regulator k_P and the damping regulator k_D. The control voltage is converted into the control current through the amplifier k_a. the dynamic displacements of the MSM rotor are measured by the displacement sensors with sensitivity coefficient k_s. The magnetic force is expressed in terms of the current stiffness and the displacement stiffness as

$$f_x = k_{ix} i_x + k_{dx} d_x \tag{10}$$

Based on the displacement feedback, the control current is

$$i_x = \left(k_P + k_D s\right) k_a k_s \cdot d_x \tag{11}$$

Substituting (11) into (10), the magnetic force is rewritten as

$$f_x = \left(k_{ix} k_P k_a k_s + k_{dx}\right) \cdot d_x + k_{ix} k_D k_a k_s \cdot \dot{d}_x \tag{12}$$

Therefore, the transfer function of the translational control loop could be written as

$$G_t(s) = \frac{k_a k_s k_i k_D s + k_a k_s k_i k_P + k_d}{m s^2 + k_a k_s k_i k_D s + k_a k_s k_i k_P + k_d} \tag{13}$$

3.2. Control Loop of Rotation

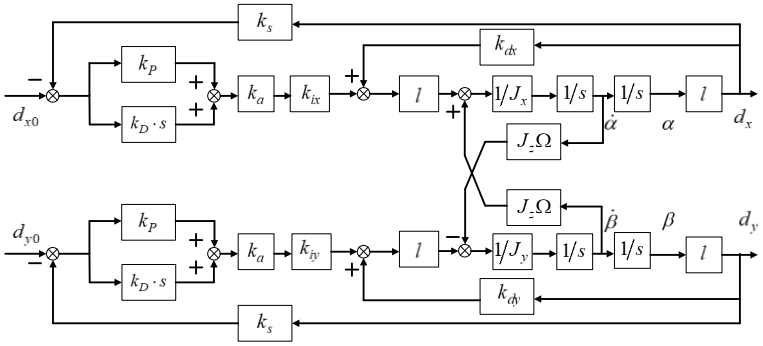

Fig. 7. The control scheme of radial rotation.

Tilting torques generated by the radial AMBs at top-end and bottom-end are used to control radial rotations of the MSM rotor, the control loop of radial rotation is shown in Fig. 7. Gyroscopic coupling terms are introduced

in radial rotations of the MSM rotor, and they vary with the rotational speed of the MSM rotor around the axial principal axis.

Substituting (3), (4) and (12) into (2), there are

$$\begin{cases} J_y\ddot{\beta} - J_z\Omega\dot{\alpha} + 2k_d l^2\beta = -2k_a k_s k_i\left(k_P\beta + k_D\dot{\beta}\right)l^2 \\ J_x\ddot{\alpha} + J_z\Omega\dot{\beta} + 2k_d l^2\alpha = -2k_a k_s k_i\left(k_P\alpha + k_D\dot{\alpha}\right)l^2 \end{cases} \tag{14}$$

The rotational angle around radial axis is defined as the form of complex number

$$\varphi(s) = \alpha(s) + \beta(s)\, j \tag{15}$$

The first equation in (14) multiplies imaginary unit j, and then add with the second equation in (14), there is

$$J_x\varphi(s)s^2 - jJ_z\Omega\varphi(s)s + 2k_d l^2\varphi(s) = -2k_a k_s k_i l^2\left(k_P + k_D s\right)\varphi(s) \tag{16}$$

The nominal transfer function of rotation is written as

$$G_r(s) = \frac{2k_i k_a k_s\left(k_P + k_D s\right)l^2 + 2k_d l^2}{J_x s^2 - jJ_z\Omega s + 2k_i k_a k_s\left(k_P + k_D s\right)l^2 + 2k_d l^2} \tag{17}$$

3.3. Robust Control Scheme

A. Control Function Synthesis for Translation

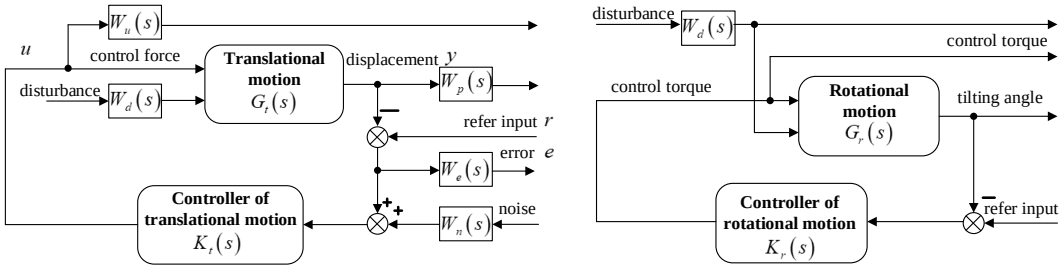

(a) (b)

Fig. 8. (a) The robust control scheme of translation, (b) The robust control scheme of radial rotation.

For translational motion of the MSM rotor, the robust control function $K_t(s)$ in Fig. 8(a) is designed to attenuate the model uncertainties due to the current stiffness and the displacement stiffness. $G_t(s)$ is transfer function. $K_t(s)$ is control function. $W_n(s)$ is transfer function of sensor noise. $W_d(s)$ is transfer function of external disturbance. $W_e(s)$ is performance weight function to evaluate control performance. $W_u(s)$ is input weight function, and $W_p(s)$ is output weight function. The nominal transfer functions $G_t(s)$ and $G_r(s)$ satisfy

$$\begin{cases} \lim\limits_{s\to\infty} G_t(s) = 0 \\ \lim\limits_{s\to\infty} G_r(s) = 0 \end{cases} \tag{18}$$

Therefore, the closed-loop transfer functions of both translation and rotation are bounded. For the controller synthesis of translation, the closed-loop transfer functions are expressed respectively as

$$\begin{cases} S(s)=\dfrac{e}{r}=\dfrac{1}{1+G_t(s)K_t(s)}, & \textit{sensitivity function} \\ R(s)=\dfrac{u}{r}=\dfrac{K_t(s)}{1+G_t(s)K_t(s)}, & \textit{penalty sensitivity function} \\ T(s)=\dfrac{y}{r}=\dfrac{G_t(s)K_t(s)}{1+G_t(s)K_t(s)}, & \textit{complementary sensitivity function} \end{cases} \tag{19}$$

A stabilizing control function $K_t(s)$ is designed to keep the stability of closed-loop system. The enhanced object model is chosen as

$$\gamma_0 = \min \|P\|_\infty = \min \left\| \begin{matrix} W_e(s)S(s) \\ W_u(s)R(s) \\ W_p(s)T(s) \end{matrix} \right\|_\infty \tag{20}$$

It must satisfy the condition as following

$$\gamma_0 \le \gamma = \|P\|_\infty \tag{21}$$

where γ is the minimal value of optimization factor. The robustness of control system increases with the value of γ. Selection of weight functions $W_e(s)$, $W_u(s)$ and $W_p(s)$ are decided by γ.

In general, $W_e(s)$ should be a low-pass filter to suppress the low-frequency disturbance of translation, so the gain of the sensitivity function $S(s)$ would be enough small to inhibit the disturbance, and weight value would be great. In addition, $W_u(s)$ should be chosen to reduce the order of designed control function. $W_p(s)$ indicates the norm bound of multiplicative perturbation, and it should have characteristics of the high-pass filter with a high rising slope. Therefore, the gain of the sensitivity function $S(s)$ would be reduced in low frequency domain, and the gain of the complementary sensitivity function $T(s)$ would be suppressed in high frequency domain.

B. Control Function Synthesis of Rotation

The gyroscopic coupling among radial rotations changes with rotational speed around z axis, so it is regarded as a varying disturbance. Moreover, the severe vibration of the MSM along radial axes would lead to deviations of the current stiffness and the displacement stiffness from their nominal values, and then causes disturbance on radial rotations of the MSM. Therefore, as illuminated in Fig. 8(b), a mixed μ-synthesis function $K_r(s)$ is designed in the control of radial rotation, and $G_r(s)$ is the transfer function of radial rotation.

4. Numerical Simulation

4.1. Model Uncertainty Analysis of MSM Rotor

A. Uncertainty Response of Translation

This part is to analyze the influence of uncertainties about the current stiffness and the displacement stiffness,

simulation is focused on axial translation and radial rotations of the MSM rotor. Considering uncertainties of the current stiffness and the displacement stiffness in section 2.3, the varying range of the axial current stiffness is [400N/A, 500N/A], and the uncertain range of the axial displacement stiffness is [-1800N/mm, -1600N/mm]. The response curve of translation is plotted in Fig. 9. The red line is the response curve of the nominal model, and the blue lines represent the response curves of uncertain models. For the step-type response in Fig. 9(b), there is divergence between the nominal model and the uncertain model when the current stiffness and the displacement stiffness deviate from nominal values.

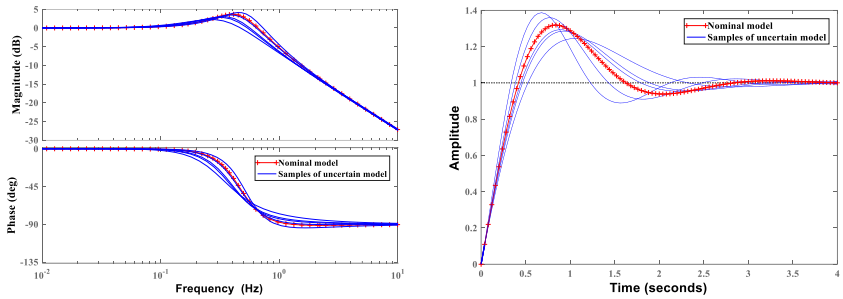

(a) (b)

Fig. 9. Response curves of axial translation, (a) frequency response, (b) step-type response.

B. Uncertainty Response of Rotation

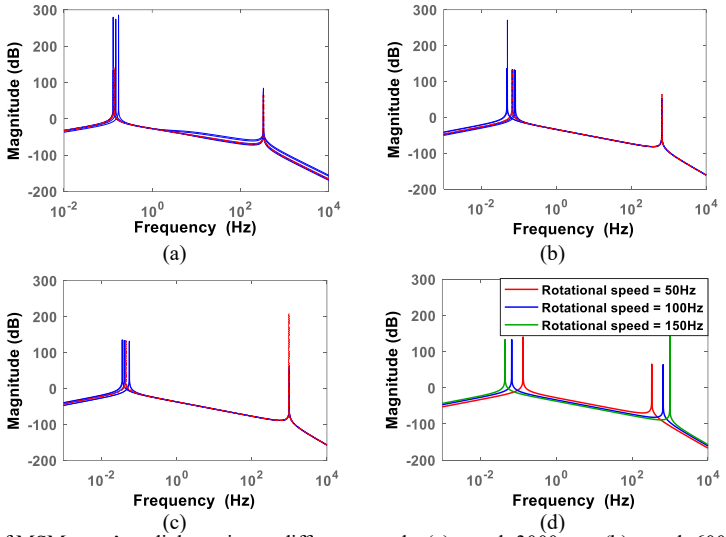

(a) (b) (c) (d)

Fig. 10. Response curves of MSM rotor's radial rotation at different speeds, (a) speed=3000rpm, (b) speed=6000rpm, (c) speed=9000rpm, (d) response of nominal model.

The uncertain range of the radial current stiffness is [600N/A, 640N/A], and the deflection range of the radial displacement stiffness is [-2900N/mm, -2700N/mm]. The response curves of radial rotation at different rotational speeds are plotted in Fig. 10. The red line is the response curve of the nominal model, and the blue lines present the response curves of MSM rotor with parameter uncertainties. The response peak at low frequency is the response magnitude of backward whirling (BW), and the response peak at high frequency is the response magnitude of

forward whirling (FW). As shown in Fig. 10(a), there are differences on the response peaks between the nominal model and the uncertain model of the MSM rotor at setting speed, so the response magnitude of uncertain model has deviation from the nominal model when the current stiffness and the displacement stiffness deviate from their nominal values. Moreover, response curves of nominal model at different speeds are depicted in Fig. 10(d), and the response amplitude varies with the rotational speed of the MSM rotor, so the comparison results show that rotational speed of the MSM rotor affects the response of radial rotation.

Moreover, the displacement deflection of the MSM rotor also varies with the rotational speed. As shown in Fig. 11(a), the displacement deflection of the MSM rotor at 4000rpm is 0.16mm, and the power spectrum density (PSD) at 67Hz is 0.075. When the rotational speed increases to 8000rpm, the displacement deflection of the MSM rotor is 0.1mm, and the PSD at 133Hz is decreased to 0.04 in Fig. 11(b), but the PSD at low frequency (6Hz) increases to 0.03. Therefore, the displacement deflection of the MSM rotor changes with rotational speed, and then the uncertainty about the current stiffness and the displacement stiffness would occur.

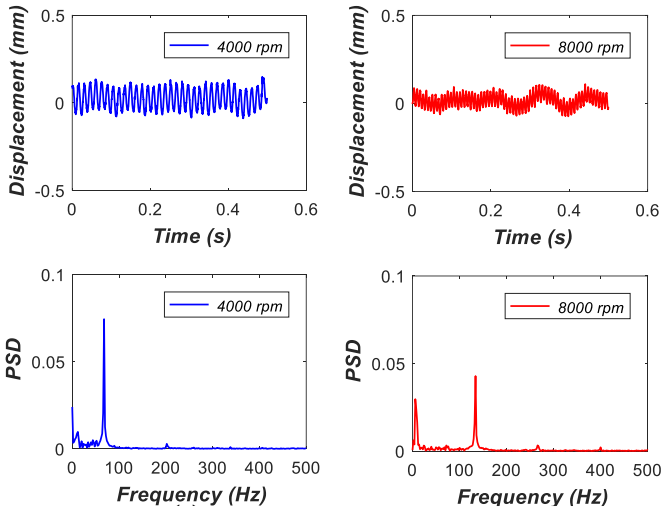

(a) (b)

Fig. 11. The displacement and PSD of the MSM rotor at different speeds, (a) speed=4000rpm, (b) speed=8000rpm.

4.2. Control Function Design

According to selection principles of the sensitivity function, the weight function and the performance function in section 3.3, for the axial translation of the MSM rotor, the input weight function, the output weight function and the performance weight function are chosen as

$$\begin{cases} W_{au}(s)=\dfrac{0.1s+10}{s+10} \\ W_{ay}(s)=\dfrac{s+500}{0.01s+100000} \\ W_{ae}(s)=\dfrac{s+5000}{0.01s+10000} \\ \gamma=0.5 \end{cases} \tag{22}$$

The control function for axial translation is chosen as

$$K_{at}(s)=\frac{0.2s^4+2.22\times10^6 s^3+2.01\times10^{12}s^2+4.3\times10^{13}s+4.29\times10^{13}}{s^5+1.01\times10^6 s^4+5.27\times10^9 s^3+1.37\times10^{12}s^2+1.38\times10^{13}s+6.34\times10^{12}} \tag{23}$$

The response magnitudes of the input weight function, the output weight function and the performance weight function in axial translation are plotted in Fig. 12(a). It indicates that the magnitude of the sensitivity function $S_a(s)$ is smaller than the magnitude of $1/W_{au}(s)$, the magnitude of the control function $R_a(s)$ is below that of $1/W_{ay}(s)$, and the magnitude of the complementary sensitivity function $T_a(s)$ is smaller than the magnitude of $1/W_{ae}(s)$.

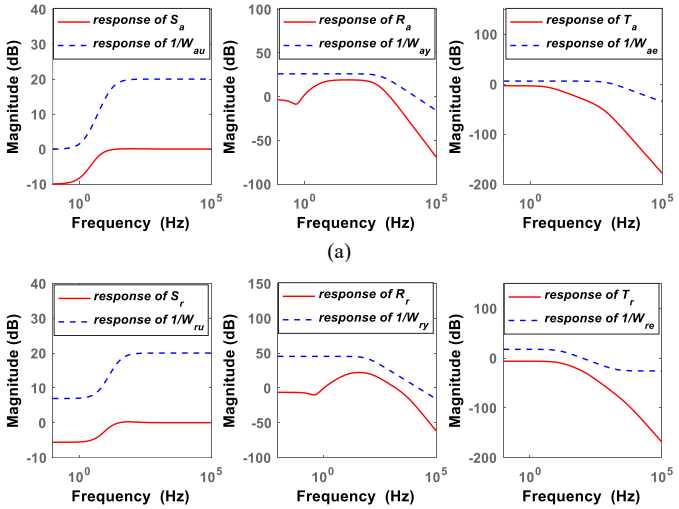

Fig. 12. (a) Response magnitude of sensitivity function, control function and complementary sensitivity function in axial translation control, (b) Response magnitude of sensitivity function, control function and complementary sensitivity function in radial translation control.

For the radial translation of the MSM rotor, the input weight function, the output weight function and the performance weight function are chosen as

$$\begin{cases} W_{ru}(s)=\dfrac{0.1s+50}{s+200} \\ W_{ry}(s)=\dfrac{s+5000}{0.01s+10000} \\ W_{re}(s)=\dfrac{s+5000}{0.01s+10000} \\ \gamma=0.2 \end{cases} \tag{24}$$

The response magnitudes of weight function and performance function are plotted in Fig. 12(b). The control

function of radial translation is designed as

$$K_{rt}(s)=\frac{0.3s^4+6.07\times10^5 s^3+3.03\times10^{11}s^2+8.01\times10^{12}s+2.53\times10^{12}}{s^5+1.01\times10^6 s^4+5.36\times10^9 s^3+1.82\times10^{12}s^2+1.58\times10^{14}s+4.95\times10^{13}} \tag{25}$$

For the radial rotation of MSM with gyroscopic coupling, the control function is designed as

$$K_r(s)=\frac{-85.18s^6-4\times10^4 s^5+8.3\times10^7 s^4+3.9\times10^{10}s^3+1.5\times10^{12}s^2+1.1\times10^{12}s+1.8\times10^{11}}{s^7+4.7\times10^2 s^6+2.2\times10^6 s^5+7.3\times10^8 s^4+6\times10^{10}s^3+5\times10^{11}s^2+2.9\times10^{11}s+4.7\times10^{10}} \tag{26}$$

Although the robust control functions in (23), (25) and (26) are both high-order equations, the programming of control functions could be realized by the high-performance digital signal processing (DSP) chip and field programmable gate array (FPGA) chip in the main processing unit (MPU).

4.3. Comparison of Control Performance

A. Control Performance of Translation

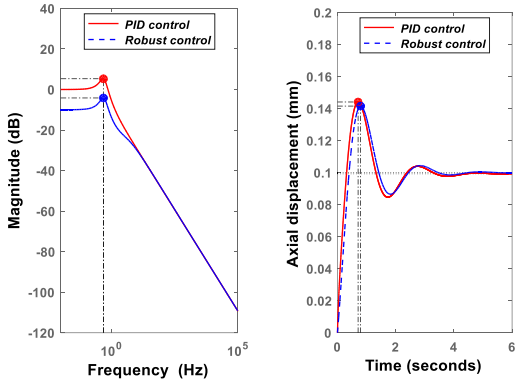

(a) (b)

Fig. 13. (a) Frequency response of axial translation, (b) step response of axial translation.

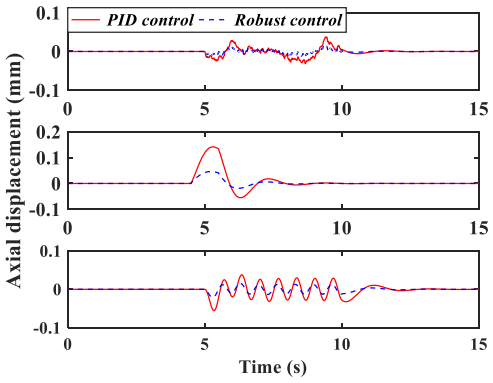

Fig. 14. Disturbance response curve of axial suspension.

Table. I. Comparison for axial suspension in simulation.

	PID Control	Robust Control	Reduction
Random disturbance	0.0187mm	0.0067mm	64.2%
Impulse disturbance	0.1416mm	0.0460mm	67.5%
Sinusoidal disturbance	0.0101mm	0.0071mm	29.7%

Although the control process of radial translation is similar to that of axial translation, the axial suspension control is more complex because the additional load is usually mounted on the axial axis of the MSM rotor, so the

control process of axial translation is chosen as the example in both simulation and experiment. The simulation is developed to compare control performances of different methods used in the axial suspension. Firstly, frequency responses of axial suspension with PID control and robust control are analyzed. As illustrated in Fig. 13(a), the response magnitude of PID control is greater than that of robust control, it means that the robust control has smaller vibration magnitude than PID control in axial translational control. Fig. 13(b) is the step-type response of axial translation, and the step-type response curve of robust control is more accurate than that of PID control, so this result proves that the robust control has better control precision in axial translation of the MSM rotor.

When the MSM rotor is stably suspended at the axial equilibrium point, dynamic displacements of the MSM rotor with PID control are plotted by the red line, and that of robust control is shown by the blue line in

Fig. 14. The random disturbance with magnitude 0.1mm is acting on the MSM rotor. The root mean square (RMS) value is the evaluation index for control performance. The RMS of PID control is 0.0187mm, and that of robust control is 0.0067mm in top figure. The response curve for pulse-type disturbance with amplitude 0.1mm is plotted in middle figure, the overshoot of PID control is 0.1416mm, and that of robust control decreases to 0.046mm. When sinusoidal-type disturbance $0.1 \cdot sin(3\pi t)$ is acting on the axial suspension of the MSM rotor, the response amplitude of PID control is 0.0101mm while that of robust control is 0.0071mm in below figure.

Based on the simulation result of axial suspension with three different disturbances, for the MSM rotor with uncertainties on the current stiffness and the displacement stiffness, the robust control has better performance on disturbance attenuation than PID control

B. Control Performance of Rotation

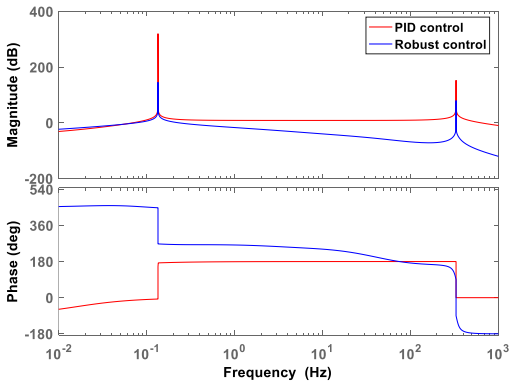

Fig. 15. Frequency response of radial rotation function.

Moreover, simulation about the rotation control of the MSM rotor is conducted. Response curves of radial rotation at 50Hz are plotted in Fig. 15. For the robust control shown by the blue line, the response magnitude of

BW at 0.5Hz is 145dB, and the response magnitude of FW at 330Hz is 77dB. In the case of PID control shown by the red line, the response magnitude of BW is 320dB, and the response magnitude of FW is 152dB. Therefore, the robust control used in the radial rotation of the MSM rotor could reduce response magnitudes of both BW and FW.

Three different disturbances are imposed on the radial rotation of the MSM rotor. The corresponding variation of rotational angle α listed in Table II is the stability index of radial rotation. Firstly, the pulse-type disturbance with amplitude 1º is applied on the radial rotation, for PID control, the peak value of rotational angle is 0.3099º, and that using robust control is 0.0914º. Secondly, the response curves for the random-type disturbance with amplitude 1º are shown in middle figure of Fig. 16. The RMS value in the case of PID control is 0.0433º while the RMS of robust control is 0.0089º. Finally, a sinusoidal-type disturbance $sin(0.4\pi t)$ is imposed on the radial rotation, and response curves are plotted in below figure of Fig. 16. The response magnitude of PID control is 0.299º , while the response magnitude of robust control is 0.2749º with the stable amplitude 0.1012º .

Based on the simulation result presented above, the robust control is more capable to suppress disturbance than PID control for axial suspension and radial rotation of the MSM rotor with uncertainties on the displacement stiffness and the current stiffness.

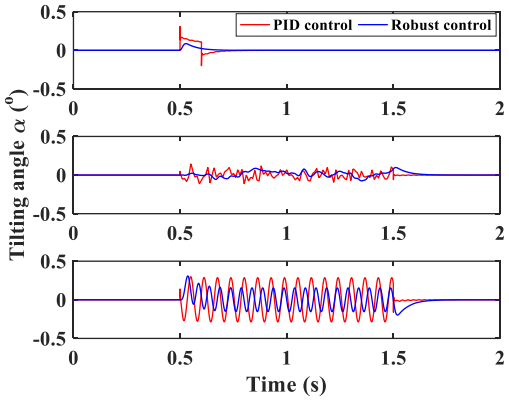

Fig. 16. Disturbance response of radial rotation.

Table II. Comparison of rotational angle with different control methods in simulation.

	PID Control	Robust Control	Reduction
Impulse disturbance	0.3099º	0.0914º	70.5%
Random disturbance	0.0443º	0.0089º	79.9%
Sinusoidal disturbance	0.2749º	0.1012º	63.2%

5. Experimental Verification

5.1. Experimental Setup

The experimental setup in Fig. 17 consists of three parts including the mechanical system, the measurement system and the control system. The mechanical system has the radial AMB, the axial AMB and the PMSM. The vacuum pump is used to reduce the wind drag when the PMSM works at a high speed, and the vacuum gauge

could measure the vacuum degree of the MSM system. The eddy current displacement sensors mounted on the stator part measure dynamic displacements of the MSM rotor. The displacement signals are amplified by charge amplifiers, and then the NI data acquisition (DAQ) PCI9655 board collects the amplified displacement signals and feedbacks to the control system. The control system contains the MPU, the DC power supply, the industrial personal computer (IPC) and the oscilloscope. The MPU based on a DSP chip (TMS320F28335) and a FPGA chip (Altera EPF10K30RC208) realizes the control algorithm programming and generates control signals, and then the plus width modulation (PWM) driving unit generates the driving current for the AMB system. The IPC timely display the working status of the MSM system such as the vacuum degree, the axial and radial displacements, the rotational speed and the winding current of AMB system. The relative parameters are listed in Table III.

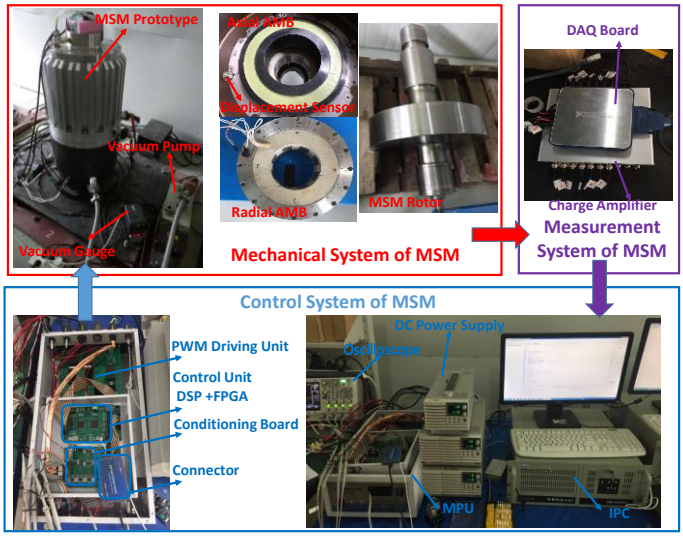

Fig. 17. Experimental setup of MSM system.

Table III. Parameters of MSM system.

Parameter	Value	Unit	Parameter	Value	Unit
Polar moment of inertia	J_z=1.477	kg·m^2	Mass of MSM rotor	m=155	kg
Equatorial moment of inertia	J_x=6.695	kg·m^2	Distance of radial sensor	l=476	mm
Radial current stiffness	k_{ix}=620	N/	Amplification coefficient	k_w=0.2	A/V
Radial displacement stiffness	k_{dx}=-2800	N/mm	Sensitivity of displacement sensor	k_s=3.3	V/mm
Axial current stiffness	k_{iz}=470	N/A	Power supply of control system	28	V
Axial displacement stiffness	k_{dz}=-1700	N/mm	DC power supply of AMB	2	A
Rated rotational speed	7800	rpm	Sampling frequency	20	KHz
Proportional coefficient of radial control	20.4		Derivative coefficient of radial control	6.2	
Proportional coefficient of axial control	13.6		Derivative coefficient of axial control	9.3	

5.2. Stable Suspension of MSM Rotor in Axial Direction

In the experiment on axial suspension, the axial displacement of the MSM rotor is zero when it is stably suspended at the axial equilibrium position. The loads with different weights are mounted on the MSM rotor in axial direction, and magnetic forces would push the MSM rotor back to the axial equilibrium position based on

displacement feedback when it deflects from the equilibrium point. The displacement deflection (difference between the maximum displacement and the minimum displacement) is used to evaluate the response magnitude of the MSM rotor. In Fig. 18, the response curve of PID control is shown by the red line, and the response curve of robust control is shown by the blue line. In middle figure of Fig. 18, a load of 20kg is added on the MSM rotor, the displacement deflection of PID control is 0.55mm, and that of robust control is 0.38mm. When a load of 40kg is added on the MSM rotor, the displacement deflection of PID control is 0.63mm, but that in the case of robust control is 0.4mm. Moreover, when a load with 60kg is added on the MSM rotor, the displacement deflection of PID control is 0.95mm, and that of robust control is decreased to 0.53mm.

Therefore, the comparison between displacement deflection of PID control and robust control is listed in Table IV, it indicates that the robust control is more effective on suppressing the disturbance acting on axial suspension of the MSM rotor than PID control.

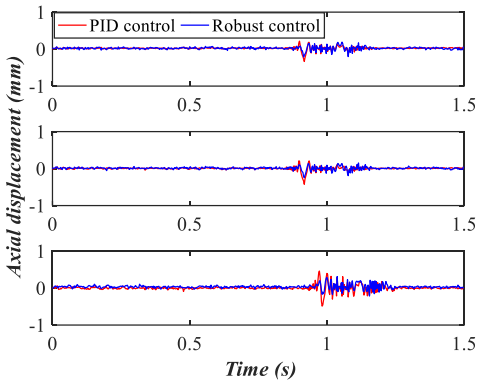

Fig. 18. Axial suspension of MSM with different loads.

Table IV. Performance comparison of axial suspension with different loads and control methods.

	PID Control	Robust Control	Reduction
Weight of load=20kg	0.55mm	0.38mm	30.9%
Weight of load=40kg	0.63mm	0.40mm	36.5%
Weight of load=60kg	0.95mm	0.53mm	44.2%

5.3. Suspension Process of MSM Rotor

The MSM rotor is forced to suspend at the axial equilibrium point, and the overshoot amount and the settling time are evaluation indices of control performance. As illustrated in Fig. 19(a), when the load with 20kg is added on the MSM rotor, the overshoot of PID control is 0.19mm, and that of robust control is 0.12mm. Fig. 19(b) shows the axial suspension trace of the MSM rotor with a 40kg load. The overshoot of PID control is 0.26mm, and that of robust control is 0.18mm. Finally, the axial suspension trace of the MSM rotor with a 60kg load is shown in Fig. 19(c). The overshoot of PID control is 0.3mm, but that of robust control decreases to 0.26mm. In addition,

the partial enlarged details of axial suspension trace are shown in Fig. 19(d), the settling time of axial suspension increases with the weight of load imposed on the MSM rotor. Therefore, based on the comparison in Table. V, the robust control has better performance on controlling axial suspension of the MSM rotor than PID control.

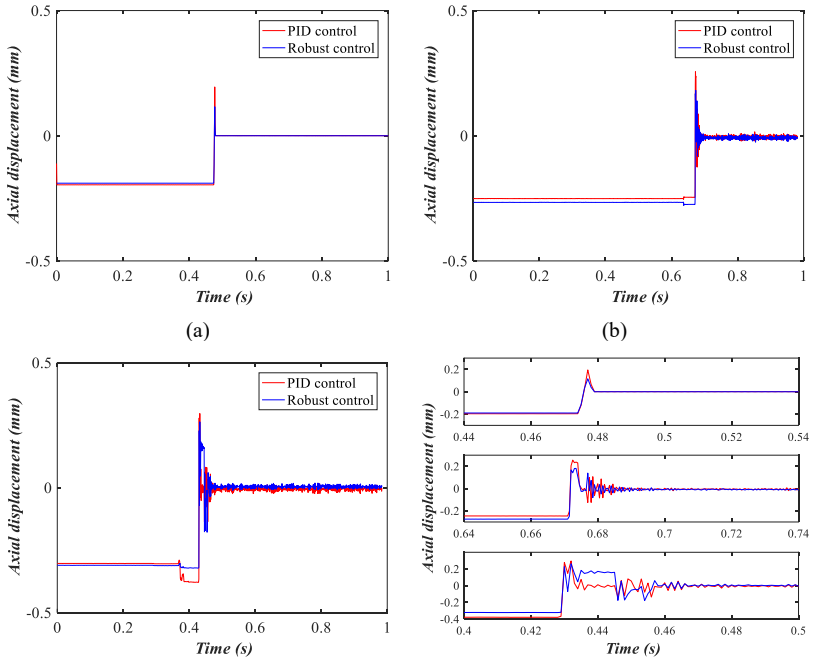

Fig. 19. Axial suspension traces of the MSM rotor with different loads, (a) weight of load=20kg, (b) weight of load=40kg, (c) weight of load=60kg, (d) stable suspension.

Table. V. Comparison of axial suspension process with different loads and control methods.

	PID Control	Robust Control	Reduction
Weight of load=20kg	0.19mm	0.12mm	36.8%
Weight of load=40kg	0.26mm	0.18mm	30.8%
Weight of load=60kg	0.30mm	0.26mm	13.3%

5.4. Disturbance Attenuation of Rotation

The control performance on radial rotation is also analyzed, and the displacement deflection from the radial equilibrium point is used to evaluate the control performance. In Fig. 20(a), a pulse-type disturbance generated by the impact hammer with amplitude 10N is imposed on the MSM rotor when the rotational speed is 2000rpm. The blue line is the radial displacement with robust control, and the red line is the radial displacement with PID control. The displacement deflection of PID control is 0.38mm, and that of robust control is 0.24mm, so the relative reduction is 36.8%. The radial displacements of MSM rotor with the pulse-type disturbance are plotted in Fig. 20(b) when the rotational speed increases to 4000rpm. The displacement deflection of PID control is 0.97mm, and that of robust control is 0.7mm, so the relative reduction is 27.8%. The radial displacements are shown in Fig. 20(c) when the rotational speed increases to 6000rpm. The displacement deviation of PID control is 0.67mm, and that of robust control is 0.52mm, so the relative reduction is 22.4%. Finally, the displacement deflection of PID

control is 0.55mm at the rated speed 8000rpm, and that of robust control is 0.48mm, the relative reduction is 12.7%.

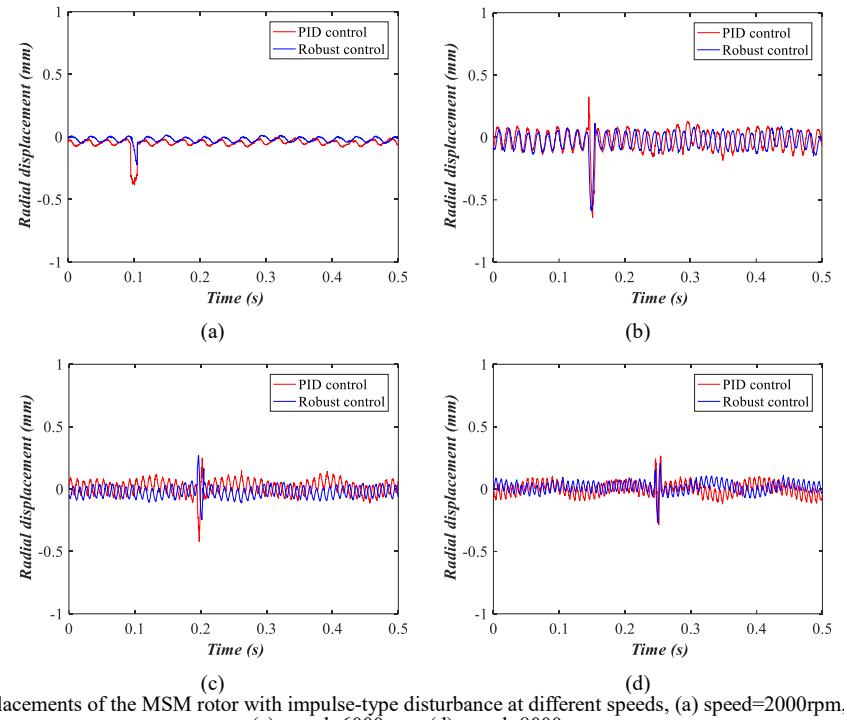

Fig. 20. Radial displacements of the MSM rotor with impulse-type disturbance at different speeds, (a) speed=2000rpm, (b) speed=4000rpm, (c) speed=6000rpm, (d) speed=8000rpm.

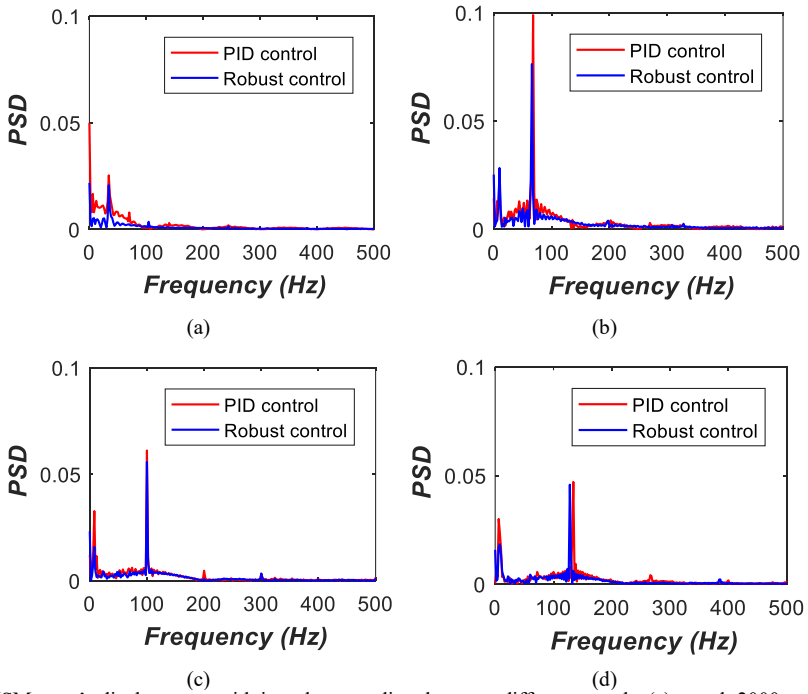

Fig. 21. PSD of the MSM rotor's displacement with impulse-type disturbance at different speeds, (a) speed=2000rpm, (b) speed=4000rpm, (c) speed=6000rpm, (d) speed=8000rpm.

Moreover, the PSD of the radial displacement is plotted in Fig. 21. When the rotational speed of the MSM rotor is 2000rpm in Fig. 21(a), the PSD with PID control is 0.025, and the PSD with robust control decreases to 0.02. The rotational speed increases to 8000rpm in Fig. 21(d), the PSD with PID control at 134Hz is 0.047, and

PSD with robust control is 0.045. Consequently, the robust control is more effective on suppressing the disturbance acting on rotation of MSM rotor than PID control.

Table VI. Comparison of radial displacement with disturbances.

	PID Control	Robust Control	Reduction
Speed=2000rpm	0.38mm	0.24mm	36.8%
Speed=4000rpm	0.97mm	0.70mm	27.8%
Speed=6000rpm	0.67mm	0.52mm	22.4%
Speed=8000rpm	0.55mm	0.48mm	12.7%
Speed-up process	0.72mm	0.52mm	27.8%

5.5. Dynamic Displacements of MSM Rotor during Speed-up

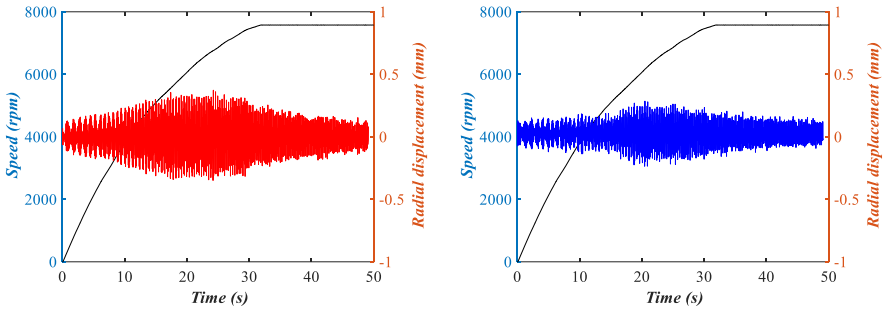

(a) (b)

Fig. 22. Dynamic displacement of MSM rotor during speed-up, (a) PID control, (b) robust control.

Finally, the dynamic displacements of the MSM rotor during speed-up process are plotted in Fig. 22 when the rotational speed is accelerated from zero to the rate speed. The radial displacement approaches to a constant value when the rotational speed of the MSM rotor approaches to the rated speed. The maximum displacement deviation of PID control is about 0.72mm in Fig. 22(a). In the case of robust control, the maximum displacement deviation is 0.52mm in Fig. 22(b). Therefore, the robust control can keep the MSM rotor more stable than PID control during the speed-up process.

6. Conclusion

The initial suspension position of the MSM rotor affects the current stiffness and the displacement stiffness, and then its suspension process is affected. Moreover, external disturbances acting on the MSM rotor also affect the nominal values of the current stiffness and the displacement stiffness. Therefore, robust control functions are designed to attenuate the disturbance for translation and radial rotation respectively. When the pulse-type, the sinusoidal-type and the random-type disturbances are respectively imposed on the MSM rotor, simulation results indicate that the robust control is more useful on suppressing the disturbance response of the MSM rotor. Experimental results show that the displacement deflection of MSM rotor with robust control is smaller at different speeds. Even though the proposed robust model has a high demand on the MPU system, it is potential to be used to improve the control stability of MSM rotor with heavy self-weight and great moment of inertia. Furthermore,

the future work would be focused on improving the control precision of the MSM with the small current and the low power consumption strategy, and the structure of the control model would be simplified to reduce the high demand on the MPU system.

Acknowledgement

This work is supported by The Hong Kong Polytechnic University [grant number CRG RUMT16900506r].

Reference

[1] M. Ahrens, L. Kucera, R. Larsonneur, Performance of a magnetically suspended flywheel energy storage device, IEEE Transactions on control systems technology, 4 (1996) 494-502.

[2] T.D. Nguyen, K.-J. Tseng, S. Zhang, H.T. Nguyen, A novel axial flux permanent-magnet machine for flywheel energy storage system: Design and analysis, IEEE transactions on Industrial Electronics, 58 (2011) 3784-3794.

[3] H. Akagi, H. Sato, Control and performance of a doubly-fed induction machine intended for a flywheel energy storage system, IEEE Transactions on Power Electronics, 17 (2002) 109-116.

[4] G.L. Agrawal, Foil air/gas bearing technology—an overview, in: ASME 1997 international gas turbine and aeroengine congress and exhibition, American Society of Mechanical Engineers, 1997, pp. V001T004A006-V001T004A006.

[5] C.-C. Wang, Application of a hybrid method to the nonlinear dynamic analysis of a flexible rotor supported by a spherical gas-lubricated bearing system, Nonlinear Analysis: Theory, Methods & Applications, 70 (2009) 2035-2053.

[6] D.M. Harris, J.W. Bush, Generating uniaxial vibration with an electrodynamic shaker and external air bearing, Journal of Sound and Vibration, 334 (2015) 255-269.

[7] H. Ma, H. Li, X. Zhao, H. Niu, B. Wen, Effects of eccentric phase difference between two discs on oil-film instability in a rotor–bearing system, Mechanical Systems and Signal Processing, 41 (2013) 526-545.

[8] W. Jianmei, K. Jianfeng, Z. Yanjuan, H. Xunjie, Viscosity monitoring and control on oil-film bearing lubrication with ferrofluids, Tribology International, 75 (2014) 61-68.

[9] J. Tang, B. Xiang, Y. Zhang, Dynamic characteristics of the rotor in a magnetically suspended control moment gyroscope with active magnetic bearing and passive magnetic bearing, ISA transactions, 53 (2014) 1357-1365.

[10] B. Xiang, J. Tang, Suspension and titling of vernier-gimballing magnetically suspended flywheel with conical magnetic bearing and Lorentz magnetic bearing, Mechatronics, 28 (2015) 46-54.

[11] G. Schweitzer, E.H. Maslen, Magnetic bearings: theory, design, and application to rotating machinery, Springer Berlin, 2009.

[12] P. Tsiotras, H. Shen, C. Hall, Satellite attitude control and power tracking with energy/momentum wheels, Journal of Guidance, Control, and Dynamics, 24 (2001) 23-34.

[13] J. Fausz, B. Wilson, C. Hall, D. Richie, V. Lappas, Survey of technology developments in flywheel attitude control and energy storage systems, Journal of guidance, control, and dynamics, 32 (2009) 354-365.

[14] B. Han, Q. Xu, Q. Yuan, Multiobjective optimization of a combined radial-axial magnetic bearing for magnetically suspended compressor, IEEE Transactions on Industrial Electronics, 63 (2016) 2284-2293.

[15] S. Zheng, R. Feng, Feedforward compensation control of rotor imbalance for high-speed magnetically suspended centrifugal compressors using a novel adaptive notch filter, Journal of Sound and Vibration, 366 (2016) 1-14.

[16] S.-M. Yang, M.-S. Huang, Design and implementation of a magnetically levitated single-axis controlled axial

blood pump, IEEE Transactions on Industrial Electronics, 56 (2009) 2213-2219.
[17] T. Masuzawa, S. Ezoe, T. Kato, Y. Okada, Magnetically suspended centrifugal blood pump with an axially levitated motor, Artificial organs, 27 (2003) 631-638.
[18] T. Masuzawa, T. Kita, K.i. Matsuda, Y. Okada, Magnetically Suspended Rotary Blood pump with radial type combined motor-bearing, Artificial Organs, 24 (2000) 468-474.
[19] B. Xiang, W. on Wong, Vibration characteristics analysis of magnetically suspended rotor in flywheel energy storage system, Journal of Sound and Vibration, 444 (2019) 235-247.
[20] M. Chen, C.R. Knospe, Control approaches to the suppression of machining chatter using active magnetic bearings, IEEE Transactions on control systems technology, 15 (2007) 220-232.
[21] B. Polajžer, J. Ritonja, G. Štumberger, D. Dolinar, J.-P. Lecointe, Decentralized PI/PD position control for active magnetic bearings, Electrical Engineering, 89 (2006) 53-59.
[22] T. Schuhmann, W. Hofmann, R. Werner, Improving operational performance of active magnetic bearings using Kalman filter and state feedback control, IEEE Transactions on Industrial Electronics, 59 (2012) 821-829.
[23] Y. Park, Design and implementation of an electromagnetic levitation system for active magnetic bearing wheels, IET Control Theory & Applications, 8 (2014) 139-148.
[24] H. Du, N. Zhang, J.C. Ji, W. Gao, Robust fuzzy control of an active magnetic bearing subject to voltage saturation, IEEE transactions on control systems technology, 18 (2010) 164-169.
[25] P.-Y. Couzon, J. Der Hagopian, Neuro-fuzzy active control of rotor suspended on active magnetic bearing, Journal of Vibration and Control, 13 (2007) 365-384.
[26] S. Sivrioglu, Adaptive backstepping for switching control active magnetic bearing system with vibrating base, IET Control Theory & Applications, 1 (2007) 1054-1059.
[27] F. Betschon, C.R. Knospe, Reducing magnetic bearing currents via gain scheduled adaptive control, IEEE/ASME transactions on mechatronics, 6 (2001) 437-443.
[28] H.S. Zad, T.I. Khan, I. Lazoglu, Design and adaptive sliding-mode control of hybrid magnetic bearings, IEEE Transactions on Industrial Electronics, 65 (2018) 2537-2547.
[29] S.-Y. Chen, F.-J. Lin, Robust nonsingular terminal sliding-mode control for nonlinear magnetic bearing system, IEEE Transactions on Control Systems Technology, 19 (2011) 636-643.
[30] S. Sivrioglu, K. Nonami, Sliding mode control with time-varying hyperplane for AMB systems, IEEE/ASME Transactions On Mechatronics, 3 (1998) 51-59.
[31] A. Noshadi, J. Shi, W.S. Lee, P. Shi, A. Kalam, Robust control of an active magnetic bearing system using H∞ and disturbance observer-based control, Journal of Vibration and Control, 23 (2017) 1857-1870.
[32] A. Noshadi, J. Shi, W.S. Lee, P. Shi, A. Kalam, System identification and robust control of multi-input multi-output active magnetic bearing systems, IEEE Transactions on control Systems technology, 24 (2016) 1227-1239.
[33] A.H. Pesch, A. Smirnov, O. Pyrhönen, J.T. Sawicki, Magnetic Bearing Spindle Tool Tracking Through ${\mu} $-Synthesis Robust Control, IEEE/ASME Transactions on Mechatronics, 20 (2015) 1448-1457.
[34] S.-L. Chen, C.-C. Weng, Robust control of a voltage-controlled three-pole active magnetic bearing system, IEEE/ASME Transactions on Mechatronics, 15 (2010) 381-388.
[35] Z. Gosiewski, A. Mystkowski, Robust control of active magnetic suspension: analytical and experimental results, Mechanical Systems and Signal Processing, 22 (2008) 1297-1303.
[36] D.H. Lee, J.B. Park, Y.H. Joo, K.C. Lin, C.H. Ham, Robust H∞ control for uncertain nonlinear active magnetic bearing systems via Takagi-Sugeno fuzzy models, International Journal of Control, Automation and Systems, 8 (2010) 636-646.

[37] H.M.N.K. Balini, C.W. Scherer, J. Witte, Performance Enhancement for AMB Systems Using Unstable H_{∞} Controllers, IEEE Transactions on Control Systems Technology, 19 (2011) 1479-1492.
[38] İ.S. Kuseyri, Robust control and unbalance compensation of rotor/active magnetic bearing systems, Journal of Vibration and Control, 18 (2012) 817-832.